Zeolitic Imidazolate Frameworks as Solid-State Nanomachines

Joohan Nam[1], Seokjin Kim[1], Eunji Jin[1], Soochan Lee[1], Hye Jin Cho[1], Seung Kyu Min[*,1,2], and Wonyoung Choe[*,1,3]

[1]Department of Chemistry, Ulsan National Institute of Science and Technology (UNIST), Ulsan 44919, Republic of Korea.

[2]Center for Multidimensional Carbon Materials (CMCM), Institute for Basic Science (IBS), Ulsan 44919, Republic of Korea.

[3]Graduate School of Carbon Neutrality, Ulsan National Institute of Science and Technology (UNIST), Ulsan 44919, Republic of Korea.

[*]Correspondence: skmin@unist.ac.kr and choe@unist.ac.kr

Abstract

Machines have continually developed with the needs of daily life and industrial applications. While the careful design of molecular-scale devices often displays enhanced properties along with mechanical movements, controlling mechanics within solid-state molecular structures remains a significant challenge. Here, we explore the distinct mechanical properties of zeolitic imidazolate frameworks (ZIFs) – frameworks that contain hidden mechanical components. Using a combination of experimental and theoretical approaches, we uncover the machine-like capabilities of ZIFs, wherein connected composite building units (CBUs) operate similarly to a mechanical linkage system. Importantly, this research suggests that certain ZIF subunits act as core mechanical components, paving an innovative view for the future design of solid-state molecular machines.

Main

Machines, defined by the interplay of links and joints that enable mechanical motion, have experienced significant evolution over time.[1] This evolution, deeply rooted in history, has met crucial demands in both civil and defense sectors, covering areas from architectural to mechanical engineering.[2–5] The foundational principles of machine design are based on the fact that their mechanical behaviors arise from a set of mechanical components,[6] such as Watt,[7] Scott-Russell,[8] Sarrus,[9] Bennett,[10] Hoberman,[11] and Klann linkages (Figure 1A).[12] Each linkage offers unique mobility, essential for machine function.[13] Machines have also evolved in various scales, now extending to the molecular level.[14] Notably, molecular machines are composed of stators and rotors, which their linkages determine the operation and functions (Figure 1B).[15] The growing list of these molecular machines, which includes robotic arms,[16] turnstiles,[17] gears,[18] shuttles,[19] elevators,[20] ratchets,[21] motors,[22] and pumps,[23] highlights their importance in areas such as nano[24] and soft robotics,[25] molecular transport,[26] and catalysis.[27] However, developing solid-state nanomachines with complex mechanical linkages remains an important challenge.[28]

We aim to utilize ZIFs,[29] a notable subclass of metal–organic frameworks (MOFs) similar to zeolites, for machine-like functions in the solid-state. Due to their ability to deform[30] and their varied topologies,[31] ZIFs can be an ideal basis for designing nanoscale machines.

In this study, we introduce a series of ZIFs with **gis** topology that incorporates mechanical linkages, where CBUs[32] function as mechanical components. Within these ZIFs, thermal responses indicate the rigidity of CBUs and highlight Zn atomic sites as crucial joints, resulting in the unique corotating movement. Additionally, the type of functional groups in imidazolate linkers can significantly influence this ZIF mechanics. This distinct mechanical feature, allowing selective deformation in **gis**-ZIFs, leads to anisotropic mechanical properties. Notably,

3

this ZIF mechanics is similar to slider-crank mechanism,[33,34] which are not belonged to traditional flexible MOFs.[35] We expect that these ZIF machines, leveraging specific mechanical components, hold the potential to reshape the field of adaptable solids, offering exceptional machinery functions.

4
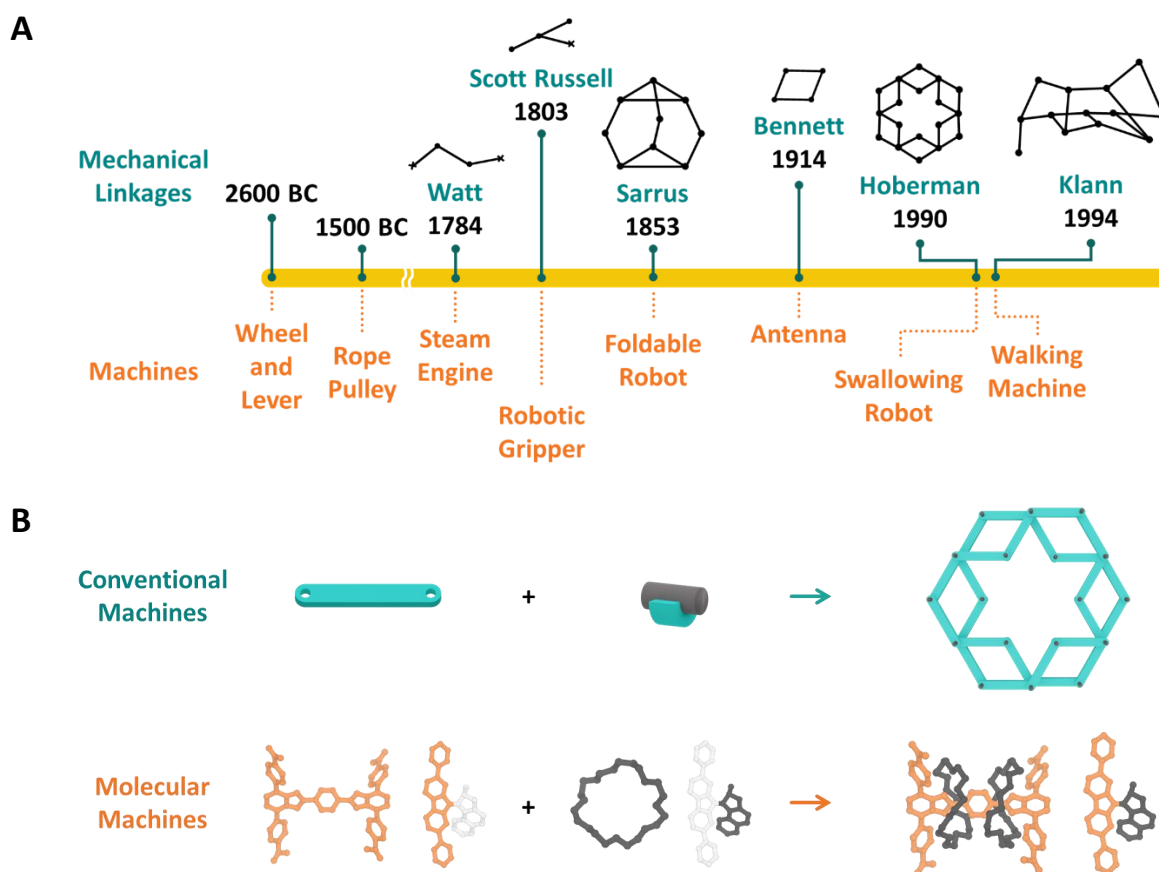
Figure 1. Historical overview for mechanical linkages and machines. (A) A brief history of mechanical linkages (top) and related machines (bottom).[7–12,36,37] (B) Mechanical components (left) and their assemblies, called machines (right). Conventional machines are composed of links and joints, and molecular machines are composed of stators and rotors.[28]

5

Synthesis and structural characterization. **gis**-ZIF-1 was synthesized with $Zn(CF_3SO_3)_2$, imidazole ligands (Im, hereafter), and ethylenediamine (EDA) in N,N-diethylformamide (DEF) solution via solvothermal reaction (Figure S1A). Single-crystal X-ray diffraction (SCXRD) revealed that **gis**-ZIF-1 is one of $Zn(Im)_2$ polymorphs[31] with **gis** topology (Figure 2A, 2B).[29,38] The **gis** topology is one of zeolitic topologies, composed of one type of tetrahedral vertices and two types of edges, where the network includes two types of CBUs, four-membered rings (4MRs) and helical chains (Figure S2A).

We noted that **gis**-ZIF-1 has distinctive structural features unlike previously reported ZIF-6.[29] In detail, ZIF-6 and **gis**-ZIF-1 have geometrically different CBUs, where 4MRs, $Zn_4(Im)_4$, are flattened squares and butterfly tetrahedra, resulting in the difference of space groups – $I4_1/amd$ (D_{4h}) in ZIF-6 and $I4_1/a$ (C_{4h}) in **gis**-ZIF-1, respectively (Figure S2B, S3). Notably, $I4_1/a$ space group is a crystallographic subgroup of $I4_1/amd$ where the reflection symmetry is eliminated and 4MRs have a rotational degree of freedom along 4_1 screw axes.

Within the unit cell, **gis**-ZIF-1 contains 16 Zn atoms interconnected by 32 Im linkers. All Zn atoms display symmetrical equivalence, and Im linkers occupy two positions of equal symmetry. Specifically, one type of Im linker forms 4MRs, while the other type constructs helical chains. These CBUs are linked through Zn atoms.

Analysis through nuclear magnetic resonance (NMR) spectroscopy revealed the presence of confined DEF solvents and the absence of EDA molecules within **gis**-ZIF-1 (Figure S4A). Notably, the tetragonal geometry of **gis**-ZIF-1 is significantly influenced by DEF solvents, as observed by the structural change upon removal of confined DEF solvents through the solvent-exchange process into MeOH (Figure S4C, S5).

Thermal response. Considering the topological sense, we expected that **gis**-ZIF-1 potentially

6

exhibits a flexible nature similar to **gis**-zeolites.[39] To confirm this structural flexibility, we performed temperature-dependent synchrotron SCXRD analysis, covering temperatures from 100K to 350K (Table S1). As temperature increased, **gis**-ZIF-1 showed anisotropic thermal expansion along a and b axes while maintaining $I4_1/a$ space group and **gis** topology. In the experiment, a and b parameters increased by 2.0 %, whereas c parameter showed a 0.2 % change (Figure 2C, S7). The volume of unit cell increased by 4.4 % from 100K to 350K, and 7.6 % from 200K to 350K (Figure 2D).

This thermal expansion was notably occurred from 200K, resembling the nonlinear expansion similar to guest-induced thermal expansion observed in MOFs.[40] The thermal expansion coefficients were calculated from the changes in cell parameters and the cell volume (Table S2, Figure S8). According to these calculations, **gis**-ZIF-1 demonstrated a colossal thermal expansion with maximum values of 690.7×10^{-6} K^{-1} for a parameter and 1709.7×10^{-6} K^{-1} for the cell volume at 200K. It is worth noting that the thermal expansion anisotropy observed in flexible materials arises from the molecular basis of expansion.[41] Therefore, we initiated a detailed exploration of the **gis**-ZIF-1 structure to identify the precise molecular movement contributing to this anisotropic thermal expansion.

7
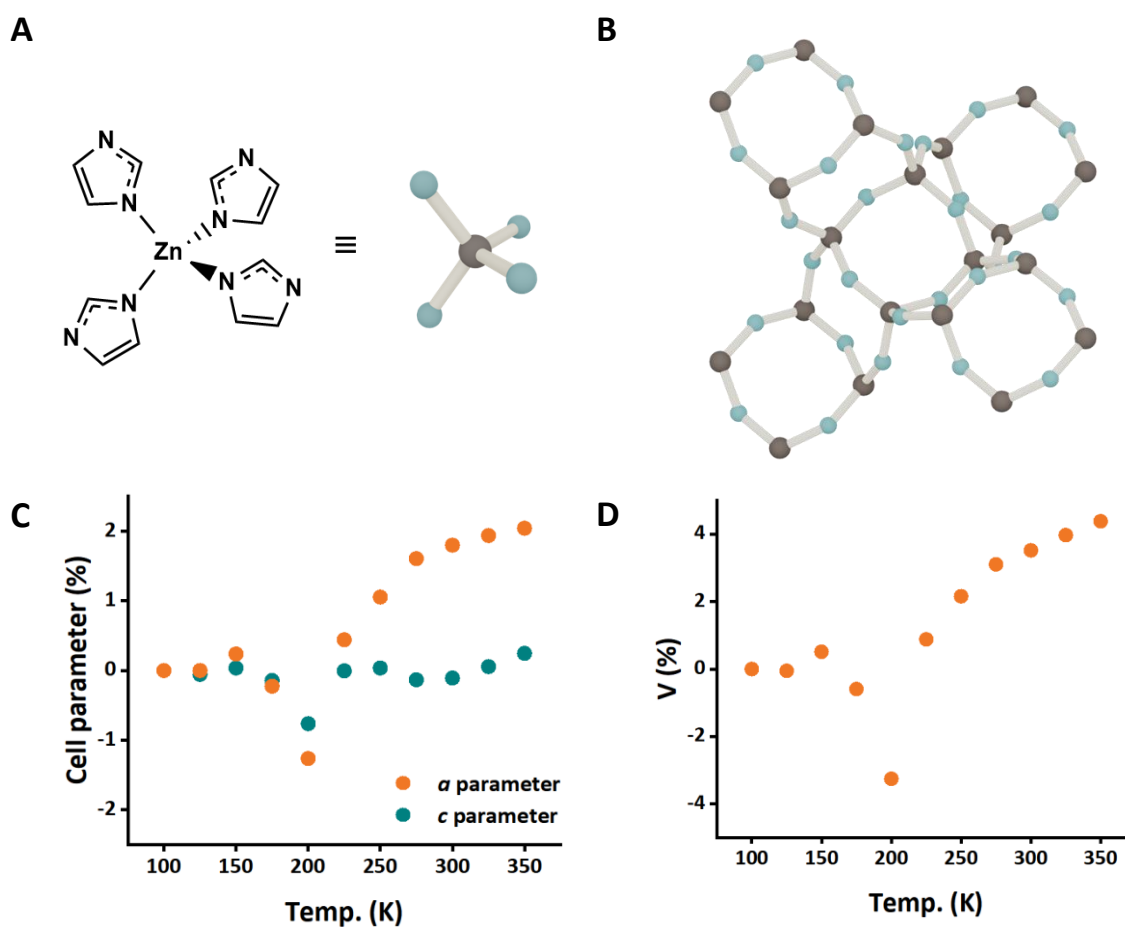
Figure 2. Structure and thermal response of gis-ZIF-1. (A) Structural similarity of tetrahedron-based ZIF and zeolite, wherein grey and light blue balls are Zn sites and centroids of imidazolate ligands. (B) Ball and stick model of **gis**-ZIF-1 single-crystal structure. Relative change of (C) a and c parameters and (D) volume of the unit cell from SCXRD (100K to 350K) data.

8

For a detailed analysis of the thermal response, we simplified the structure using a zeolite TO_2 model, where T and O sites represent the Zn atom and the centroid of the Im linker, respectively. This model contains three variables: TO length, TOT and OTO angles. Within the zeolite model of **gis**-ZIF-1, the asymmetric units are TO_2 with one type of T center and two types of O bridges, corresponding to the T_4O_4 for 4MR and T_nO_n for helical chains. We proceeded to track the distances between TO_4 tetrahedra, termed as TT lengths, finding that there are two types of symmetrically identical TT lengths, which vary depending on the type of O bridges involved. The variations in TT lengths across the temperature range were negligible, with measurement of 6.02(2) Å and 5.93(2) Å for each type, respectively (Table S3). Subsequently, we analyzed these TT lengths along three axes parallel to the unit cell, denoted as L_1 and L_2 on the *ab* plane, and L_3 along the *c* axis (Figure S10). These lengths were practically constant in the SCXRD data, with less than 2% change (Figure 3A, S9-S10, Table S4).

The data clearly showed the rigidity of CBUs, functioning as mechanical components (Figure 3B). Additionally, identifying these rigid components emphasized an important factor: the angle between 4MRs and helical chains termed as rotating angle (θ, hereafter), which altered by about 9º over the temperature range (Figure 3C, Table S4). This kind of mechanics was also observed in DMA-exchanged **gis**-ZIF-1, with 10º change of θ (Table S5, Figure S11). This selective flexibility closely resembled the behavior of mechanical linkages in conventional machines.[42] As such, **gis**-ZIF-1 exhibited machine-like operation under temperature variations. This led us to conduct a detailed exploration into the mechanics of **gis**-ZIF-1.
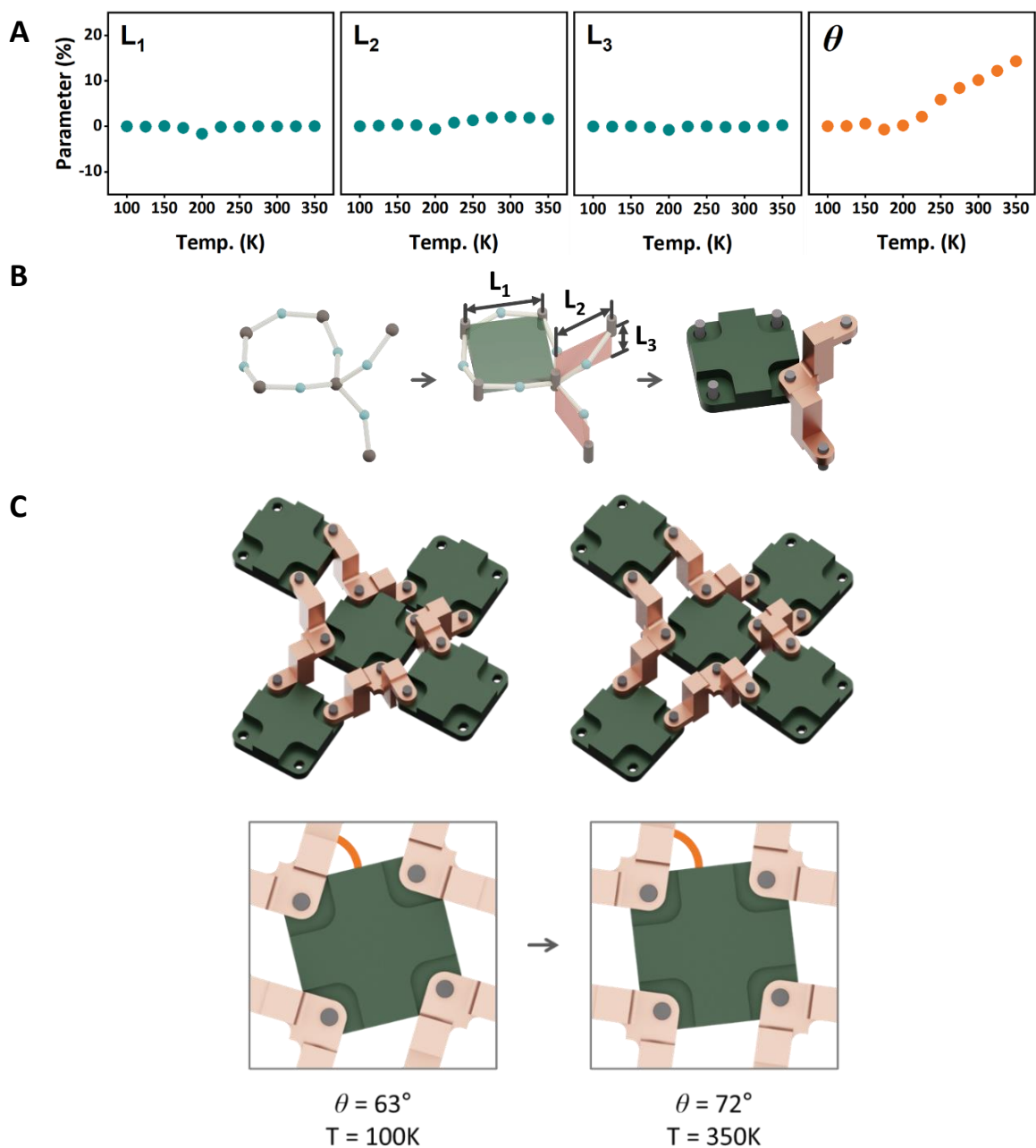
Figure 3. Mechanical model of gis-ZIF-1 structure. (A) Comparison of the changes in lengths inside rigid mechanical components, and angle between these components. (B) Representation of CBUs as mechanical components inside **gis** topology. Green components represent 4-membered rings (4MRs), copper-coloured components represent helical chains with 4_1 screw symmetry. (C) Mechanical movement of the ZIF machine, with the change of θ demonstrated in temperature-dependent SCXRD analysis.

Mathematical analysis has been consistently effective in unravelling the mechanics of various mechanical systems.[40,43] The mechanical behavior of **gis**-ZIF-1 can be thoroughly explained through a mathematical model, predominantly defined by a single variable, θ. This variable is directly linked to Cartesian coordinates, which are derived from the projection on *ab* plane within the unit cell of **gis**-ZIF-1 (Figure 4A, S12). As a result, the correlation between *a* parameter and θ can be accurately represented by a simple mathematical equation, as defined below.

$$a = 2\sqrt{L_1{}^2 + L_2{}^2 + 2L_1L_2 \sin \theta}$$

In this equation, the change of *a* parameter is directly correlated to the variation of θ without involvement of additional variables with the assumption that L_1 and L_2 remains constant, as confirmed in temperature-dependent SCXRD data. To validify this equation, we compared the calculated *a* parameter across the specified range of θ against the crystallographic data (Figure 4B). As illustrated in Figure 4B, the relationship between *a* parameter and θ aligned remarkably well with the calculated values derived from the mathematical equation (Figure 4B). We noted that this ZIF mechanics exhibits a form of rotation-correlated translation, similar to slider-crank mechanism observed in ordinary[33] and biological[34] machines. Also, using this mathematical equation and 3D printing technology, we demonstrated the macroscopic version of **gis**-ZIF-1 with the same mechanics (Figure S13).

To investigate the molecular origin of this mechanics, we conducted a direct comparison between the mechanical model and the zeolite TO_2 model of **gis**-ZIF-1. Based on the asymmetric unit TO_2, the unit cell of **gis**-ZIF-1 includes four symmetrically distinct TO lengths

11

(Table S6). These values remained nearly constant, regardless of temperature. Within the unit cell, two TOT angles, also referred to as bridging angles, were distinctive, each of them associated with the symmetry of O sites. Each TOT angle corresponds to specific mechanical components, 4MR and helical chain, respectively. TOT angles were changed by less than 1º within the 4MR components but changed by 2.9º within helical chains as the temperature increased (Table S7).

However, the OTO angles, also known as tetrahedral angles, represent the angles between the 4MR and helical chain, giving rise to six symmetrically independent OTO angles. Among these, we focused on two vertical angles to each other within the TO_4 tetrahedron. One of these angles increased by approximately 3.6º, while the other decreased by about 3.2º; the remaining four OTO angles remained rigid (Table S8, Figure S14). The position of the increased OTO angle (α, hereafter) precisely aligned with the position of the rotating angle θ, and their changes exhibited a similar trend (Figure 4C). This indicates that the molecular origin of this mechanical behavior lies in the selective deformation of the OTO angle α. In contrast, in case of **gis**-zeolites, OTO angles are more rigid than TOT angles under mechanical stimuli, resulting in different mechanisms with a constant rotating angle θ (Figure 4D).[39,44]

12
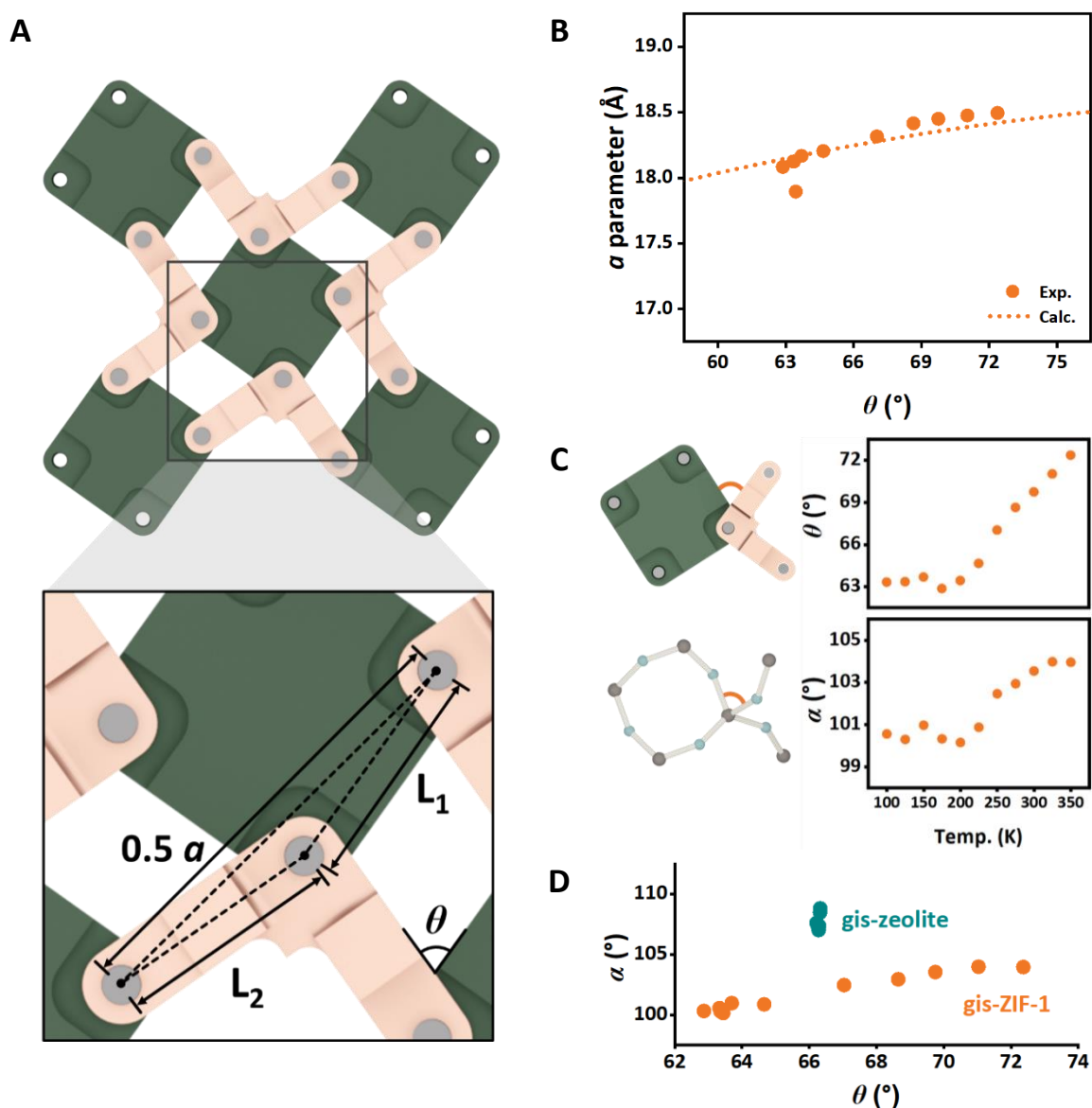
Figure 4. ZIF mechanics and its molecular origin. Mathematical analysis of ZIF mechanics with (A) 2D projected model and (B) comparison of experimental and calculated relationship between θ and a parameter. (C) Comparison of rotating angle θ and OTO angle α as function of temperature. As the temperature increased, the two types of angles (θ and α) increased. (D) Comparison of the mechanics in **gis**-ZIF-1 (this work) and **gis**-zeolite.[39]

13

Replacement of mechanical components. We further explored an additional machinery aspect within **gis**-ZIF-1 by replacing the mechanical components with bulky functional groups (Figure 5A, 5B). Our chosen candidate, **gis**-ZIF-2, is an isostructure with TIF-5[45] and belongs to the **gis**-type ZIFs. The ZIF includes the highly bulky imidazolate, 5,6-dimethylbenzimiadzolate (dmbIm, hereafter) on the helical chain. The synthesis of **gis**-ZIF-2 involved a solvothermal reaction utilizing $Zn(NO_3)_2 \cdot 6H_2O$, Im and dmbIm, with the crystal structure being confirmed through synchrotron SCXRD. Notably, **gis**-ZIF-2 was crystallized in **gis** topology with $I4_1/a$ space group, which is identical to **gis**-ZIF-1. The Im and dmbIm moieties are distinctly separated within the crystal structure, where Im constitutes 4MR components, and dmbIm forms helical chain components. In NMR spectroscopy, the ratio of Im and dmbIm was confirmed as 1:1, matched with the crystallographic ratio of 4MR and helical chain components (Figure S15). Within the unit cell, **gis**-ZIF-2 contains 16 Zn atoms interconnected by 16 Im linkers and 16 dmbIm linkers. Zn, Im, and dmbIm each occupy a single symmetrical position, respectively. We explored the thermal response of **gis**-ZIF-2 through temperature-dependent synchrotron SCXRD analysis within the temperature range 100K to 350K (Table S9). Calculated thermal expansion coefficients confirmed that the thermal expansion of **gis**-ZIF-2 is notably restrained by the presence of bulky components, with maximum values are 55.3×10^{-6} K^{-1} for *a* parameter and 91.9×10^{-6} K^{-1} for the cell volume, observed at 200K (Table S10, Figure S17). Similar to **gis**-ZIF-1, **gis**-ZIF-2 also maintains rigid components with less than 0.1 Å change across the temperature range (Table S11, Figure S18). The rotating angle θ increased by 1.4º, indicating that rotational mechanics is hindered due to the replacement of mechanical components. In terms of molecular origin, the OTO angle α increased by approximately 1.7º, roughly half of the increase observed in **gis**-ZIF-1 (Figure 5C,

14

Table S13).

To elucidate this controllable mechanics, we computed the potential energy profiles for the **gis**-ZIF series by varying the rotating angle θ (Figure 5D, S20). The simulated energy curves distinctively exhibit the difference between **gis**-ZIF-1 and **gis**-ZIF-2. The shallow curve observed for **gis**-ZIF-1 signifies the ease of rotational mechanics, whereas the steep curve of **gis**-ZIF-2 shows the hindrance in the mechanics.

15
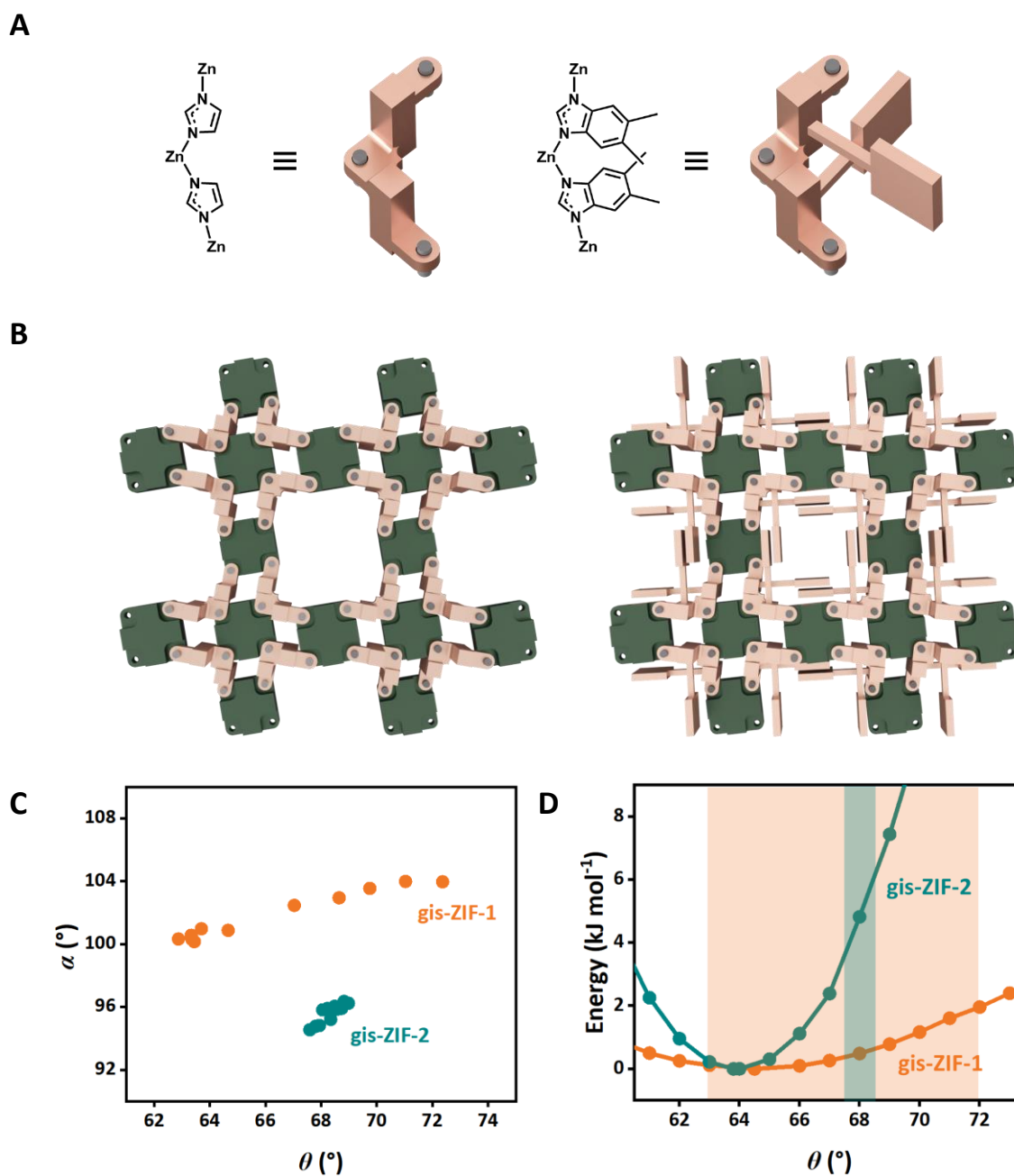
Figure 5. Controlling mechanical movement in ZIF machines. (A) Tuning the mechanical component by attaching functional groups in molecular links. (B) Extended structures of **gis**-ZIF-1 (left) and **gis**-ZIF-2 (right) at 100K. Comparison of (C) the correlation between rotating angle θ and OTO angle α, and (D) relative potential energy profile per Zn for simulated ZIF mechanics, with the range of θ in SCXRD data represented as colored regions.

16

Mechanical properties. Thus far, we demonstrated the machinery capability of **gis**-ZIF-1 based on thermal response. Therefore, we investigated its mechanical properties by theoretical calculations. Obtained elastic properties are Young's modulus (E), linear compressibility (β), shear modulus (G), and Poisson's ratio (v), calculated from elastic constants by ElaStic software (Figure 6A, Table S15).

In case of Young's modulus of **gis**-ZIF-1, the minimum value (E_{min}) is 0.84 GPa, where the deformation is along c axis, and the maximum value (E_{max}) is 1.60 GPa, where the deformation axis is perpendicular to the c axis. Young's modulus represents the compressive elasticity, which means the compression of **gis**-ZIF-1 structure is preferred perpendicular to the c axis, with anisotropy about 1.89 ($=E_{max}/E_{min}$). Linear compressibility shows similar tendency with Young's modulus, with anisotropy about 4.10 ($=\beta_{max}/\beta_{min}$). These anisotropic mechanical properties are well-matched with the anisotropic thermal response and related ZIF mechanics (Figure S23). Also, the minimum value of shear modulus (G_{min}) is 0.29, and the maximum value (G_{max}) is 0.61. Interestingly, **gis**-ZIF-1 ranks among the lowest in terms of E_{max} and G_{max} values, and the highest in terms of β_{max} compared to other published MOFs (Figure 6B, Table S17–S19).

17
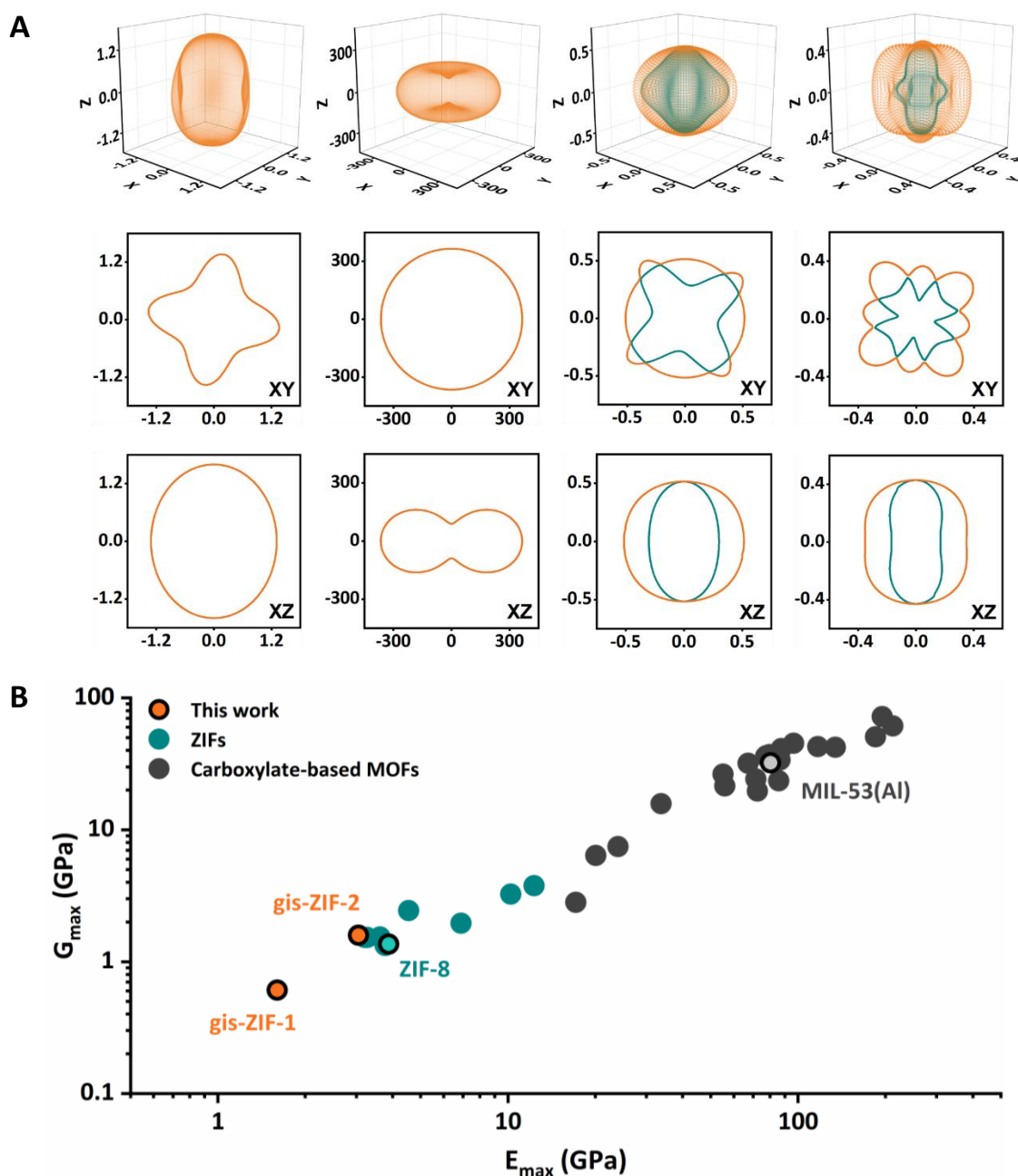
Figure 6. Calculated mechanical properties of gis-ZIF-1. 3D surface and 2D polar plots of Young's modulus, linear compressibility, maximal (orange) and minimal (green) shear modulus and Poisson's ratio. Each direction (x, y, z) represents a, b, and c parameter directions in tetragonal crystal system of **gis**-ZIF-1. (B) Relationship between maximal Young's modulus and shear modulus of MOFs (see Table S15-S20).

18

Conclusions. In summary, we report **gis**-ZIF-1 as a solid-state nanomachine, wherein CBUs function as intricate mechanical components, facilitating ZIF mechanics analogous to a slider-crank mechanism. The unique mechanics of **gis**-ZIF-1 originated from molecular movements, resulting in flexible OTO angles, markedly different from other frameworks, such as zeolites and Cu-based ZIFs (see Table S22). By employing mathematical formulations, we have precisely modeled the mechanics of **gis**-ZIF-1, resembling its macroscopic counterparts. Surprisingly, when bulky chemical functionalities are incorporated into **gis** framework, these bulky components act as stoppers, similar to those in macroscopic machines. Furthermore, **gis**-ZIF-1 exhibits exceptionally low Young's and shear moduli, representing it as a potential candidate for applications requiring energy absorption.[46]

Our findings demonstrate that ZIF nanomachines are indeed mechanical metamaterials, with their mechanical properties largely determined by the structure and connectivity of their rigid components, according to the work by Alavi *et al*.[47] Notably, the ZIF nanomachines presented here enable efficient synergistic movements between rigid components through adjustable chemical functionalities. This capability may pave a way for advancements in properties interlinked with mechanical behavior, exhibiting the vast potential in the realm of nanotechnology, including soft robotics[48] and digital data storage (see Figure S24).[49] We expect that such efforts provide a blueprint for design of solid-state nanomachines at the molecular scale.[40,43]

19

Methods

Powder X-ray diffraction (PXRD). X-ray powder diffraction data were collected on a Bruker D2 PHASER diffractometer with Cu Kα radiation (λ=1.54184 Å) and at 6D beamline in Pohang Accelerator Laboratory (PAL) with synchrotron light source (λ=0.65303 Å).

Temperature-dependent synchrotron single-crystal X-ray diffraction (SCXRD). X-ray single-crystal diffraction data were collected at 2D beamline in PAL with synchrotron light source (λ=0.7 Å). ZIF crystals were sealed in a borosilicate capillary, which diameter and wall thickness are 0.2 mm and 0.01 mm, respectively, with a small amount of mother solvents. Temperature-dependent SCXRD experiments were conducted from 100 K to 350 K at 25 K interval for **gis**-ZiF-1 and **gis**-ZIF-2. The crystallographic data was deposited in the Cambridge Crystallographic Data Centre (CCDC 2291990-2292000 for **gis**-ZIF-1, CCDC 2292005-2292015 for **gis**-ZIF-2, CCDC 2287366 and 2287487 for DMA-exchanged **gis**-ZIF-1).

^{1}H NMR. ^{1}H NMR data were collected on Agilent FT-NMR (400-MR DD2) spectrometer.

Synthesis of gis-ZIF-1. Zinc trifluoromethanesulfonate (2.908 g, 8 mmol) and imidazole (2.18 g, 32 mmol) were respectively dissolved in 40 mL of N,N-diethylformamide (DEF) solvent for making a stock solution. Then, put the 2 mL of stock solution of zinc trifluoromethanesulfonate and 1 mL of stock solution of imidazole in 10 mL vial. After that, 1 mL of additional DEF and 30 μL of ethylenediamine (0.45 mmol) were mixed in the 10 mL vial. The mixed solution was heated at 90 ℃ for 48 hours. After the reaction, colourless crystals were collected and washed with DEF.

Synthesis of gis-ZIF-2. Zinc nitrate hexahydrate (100 mg, 0.34 mmol), imidazole (65 mg, 0.95 mmol), 5,6-dimethylbenzimidazole (77 mg, 0.53 mmol) were respectively dissolved in 5 mL of N,N-dimethylformamide (DMF) solvent for making a stock solution. After then, 1 mL of each stock solution was mixed in 5 mL vial (total 3 mL of solution per vial). The mixed solution

20

was heated at 120 °C for 72 hours. After the reaction, brown crystals were collected and washed

with DMF.

21

Reference

1. Zhang, C. & Yang, J. *A History of Mechanical Engineering*. (Springer, 2020).

2. Davila Delgado, J. M., Oyedele, L., Demian, P. & Beach, T. A research agenda for augmented and virtual reality in architecture, engineering and construction. *Adv. Eng. Inform.* **45**, 101122 (2020).

3. Wickert, J. & Lewis, K. *An Introduction to Mechanical Engineering, Enhanced Edition*. (Cengage Learning, 2020).

4. Ospina-Henao, P., Carrillo-Suárez, A., Guarín-Martínez, L., Ortíz-Blanco, A. & Peñaranda-Vega, J. Partial feedback linearization for a path control in a gantry crane used in lifting machinery in civil engineering. *J. Phys. Conf. Ser.* **1723**, 012049 (2021).

5. Landa, M. D. *War in the Age of Intelligent Machines*. (Zone Books, 1991).

6. Norton, R. L. *Design of Machinery: An Introduction to the Synthesis and Analysis of Mechanisms and Machines*. (Mcgraw-Hill College, 2003).

7. Moon, F. C. Franz Reuleaux: Contributions to 19th century kinematics and theory of machines. *Appl. Mech. Rev.* **56**, 261–285 (2003).

8. Zhu, J. & Hao, G. Design and test of a compact compliant gripper using the Scott–Russell mechanism. *Arch. Civ. Mech. Eng.* **20**, 81 (2020).

9. Liu, R., Yao, Y. & Li, Y. Design and analysis of a deployable tetrahedron-based mobile robot constructed by Sarrus linkages. *Mech. Mach. Theory* **152**, 103964 (2020).

10. Chen, Y. & You, Z. On mobile assemblies of Bennett linkages. *Proc. R. Soc. Math. Phys. Eng. Sci.* **464**, 1275–1293 (2008).

11. Cai, J., Xu, Y. & Feng, J. Kinematic analysis of Hoberman's Linkages with the screw theory. *Mech. Mach. Theory* **63**, 28–34 (2013).

12. Klann, J. C. WALKING DEVICE. (2001).

22

13. McCarthy, J. M. & Soh, G. S. *Geometric Design of Linkages (Interdisciplinary Applied Mathematics, 11)*. (Springer, 2010).

14. *Molecular Robotics: An Introduction*. (Springer Nature Singapore, 2022). doi:10.1007/978-981-19-3987-7.

15. Aprahamian, I. The Future of Molecular Machines. *ACS Cent. Sci.* **6**, 347–358 (2020).

16. Kopperger, E. *et al.* A self-assembled nanoscale robotic arm controlled by electric fields. *Science* **359**, 296–301 (2018).

17. Bedard, T. C. & Moore, J. S. Design and synthesis of molecular turnstiles. *J. Am. Chem. Soc.* **117**, 10662–10671 (1995).

18. Stevens, A. M. & Richards, C. J. A metallocene molecular gear. *Tetrahedron Lett.* **38**, 7805–7808 (1997).

19. Anelli, P. L., Spencer, N. & Stoddart, J. F. A molecular shuttle. *J. Am. Chem. Soc.* **113**, 5131–5133 (1991).

20. Badjić, J. D., Balzani, V., Credi, A., Silvi, S. & Stoddart, J. F. A Molecular Elevator. *Science* **303**, 1845–1849 (2004).

21. Kelly, T. R., Tellitu, I. & Sestelo, J. P. In Search of Molecular Ratchets. *Angew. Chem. Int. Ed. Engl.* **36**, 1866–1868 (1997).

22. Koumura, N., Zijlstra, R. W. J., van Delden, R. A., Harada, N. & Feringa, B. L. Light-driven monodirectional molecular rotor. *Nature* **401**, 152–155 (1999).

23. Cheng, C. *et al.* An artificial molecular pump. *Nat. Nanotechnol.* **10**, 547–553 (2015).

24. Kassem, S. *et al.* Site-to-site peptide transport on a molecular platform using a small-molecule robotic arm. *Chem. Sci.* **12**, 2065–2070 (2021).

25. Shaik, S. & Dubey, K. D. Nanomachines in living matters: the soft-robot cytochrome P450. *Trends Chem.* **5**, 763–774 (2023).

26. Badjic, J. D. *et al.* Operating Molecular Elevators. *J. Am. Chem. Soc.* **128**, 1489–1499 (2006).

27. Corra, S. *et al.* Kinetic and energetic insights into the dissipative non-equilibrium operation of an autonomous light-powered supramolecular pump. *Nat. Nanotechnol.* **17**, 746–751 (2022).

28. Feng, L., Astumian, R. D. & Stoddart, J. F. Controlling dynamics in extended molecular frameworks. *Nat. Rev. Chem.* **6**, 705–725 (2022).

29. Park, K. S. *et al.* Exceptional chemical and thermal stability of zeolitic imidazolate frameworks. *Proc. Natl. Acad. Sci.* **103**, 10186–10191 (2006).

30. Iacomi, P. & Maurin, G. ResponZIF Structures: Zeolitic Imidazolate Frameworks as Stimuli-Responsive Materials. *ACS Appl. Mater. Interfaces* **13**, 50602–50642 (2021).

31. Lee, S., Nam, D., Yang, D. C. & Choe, W. Unveiling Hidden Zeolitic Imidazolate Frameworks Guided by Intuition-Based Geometrical Factors. *Small* **19**, 2300036 (2023).

32. Anurova, N. A., Blatov, V. A., Ilyushin, G. D. & Proserpio, D. M. Natural Tilings for Zeolite-Type Frameworks. *J. Phys. Chem. C* **114**, 10160–10170 (2010).

33. Zheng, E. & Zhou, X. Modeling and simulation of flexible slider-crank mechanism with clearance for a closed high speed press system. *Mech. Mach. Theory* **74**, 10–30 (2014).

34. Van Ingen Schenau, G. J. From rotation to translation: Constraints on multi-joint movements and the unique action of bi-articular muscles. *Hum. Mov. Sci.* **8**, 301–337 (1989).

35. Lee, J. H., Jeoung, S., Chung, Y. G. & Moon, H. R. Elucidation of flexible metal-organic frameworks: Research progresses and recent developments. *Coord. Chem. Rev.* **389**, 161–188 (2019).

36. Zhang, Y., Qian, Z., Huang, H., Yang, X. & Li, B. A Snake-Inspired Swallowing Robot Based on Hoberman's Linkages. *J. Mech. Robot.* **14**, 060905 (2022).

37. Song, X. *et al.* Networking of Bennett linkages and its application on deployable parabolic cylindrical antenna. *Mech. Mach. Theory* **109**, 95–125 (2017).

38. Tian, Y.-Q. *et al.* Design and Generation of Extended Zeolitic Metal–Organic Frameworks (ZMOFs): Synthesis and Crystal Structures of Zinc(II) Imidazolate Polymers with Zeolitic Topologies. *Chem. - Eur. J.* **13**, 4146–4154 (2007).

39. Lee, Y., Kim, S. J., Kao, C.-C. & Vogt, T. Pressure-Induced Hydration and Order−Disorder Transition in a Synthetic Potassium Gallosilicate Zeolite with Gismondine Topology. *J. Am. Chem. Soc.* **130**, 2842–2850 (2008).

40. Jin, E. *et al.* Metal-organic framework based on hinged cube tessellation as transformable mechanical metamaterial. *Sci. Adv.* **5**, eaav4119 (2019).

41. Romao, C. P. Anisotropic thermal expansion in flexible materials. *Phys. Rev. B* **96**, 134113 (2017).

42. Marghitu, D. B. *Kinematic Chains and Machine Components Design*. (Academic Press, 2005).

43. Jin, E. *et al.* Origamic metal-organic framework toward mechanical metamaterial. *Nat. Commun.* **14**, 7938 (2023).

44. Sartbaeva, A., Wells, S. A., Treacy, M. M. J. & Thorpe, M. F. The flexibility window in zeolites. *Nat. Mater.* **5**, 962–965 (2006).

45. Wu, T., Bu, X., Zhang, J. & Feng, P. New Zeolitic Imidazolate Frameworks: From Unprecedented Assembly of Cubic Clusters to Ordered Cooperative Organization of Complementary Ligands. *Chem. Mater.* **20**, 7377–7382 (2008).

46. Sun, Y. *et al.* High-rate nanofluidic energy absorption in porous zeolitic frameworks. *Nat. Mater.* **20**, 1015–1023 (2021).

47. Jiao, P., Mueller, J., Raney, J. R., Zheng, X. & Alavi, A. H. Mechanical metamaterials and beyond. *Nat. Commun.* **14**, 6004 (2023).

48. Rafsanjani, A., Bertoldi, K. & Studart, A. R. Programming soft robots with flexible mechanical metamaterials. *Sci. Robot.* **4**, eaav7874 (2019).

49. El Helou, C., Buskohl, P. R., Tabor, C. E. & Harne, R. L. Digital logic gates in soft, conductive mechanical metamaterials. *Nat. Commun.* **12**, 1633 (2021).

Author Information

Corresponding Authors

*e-mail: skmin@unist.ac.kr and choe@unist.ac.kr

ORCID

Joohan Nam: 0000-0001-5123-418X

Seokjin Kim: 0000-0001-5733-1626

Eunji Jin: 0000-0002-2103-6526

Soochan Lee: 0000-0002-1533-3727

Hye Jin Cho: 0000-0002-2365-0618

Seung Kyu Min: 0000-0001-5636-3407

Wonyoung Choe: 0000-0003-0957-1187

Contributions

Conceptualization, J.N. and W.C.; Methodology, J.N., H.J.C. and W.C.; Crystal structure analysis, J.N. and E.J.; Simulation, S.K. and S.K.M.; Property Characterization, J.N., S.L. and H.J.C.; Writing–Review & Editing, J.N., S.K., S.K.M., and W.C.

Competing interests

The authors declare no competing financial interest.

Data availability

All data are available in the Article or Supplementary Information.

Acknowledgements